Supporting Information for

Lithographically defined crosslinkable top-coats for nano-manufacturing with high-χ block copolymers

Xavier Chevalier,[1,] Cindy Gomes Correia,[2] Gwenaelle Pound-Lana,[3] Philippe Bézard,[3,†] Matthieu Sérégé,[3] Camille Petit-Etienne,[3] Guillaume Gay,[3] Gilles Cunge,[3] Benjamin Cabannes-Boué,[2] Célia Nicolet,[1] Christophe Navarro,[1] Ian Cayrefourcq,[1,‡], Marcus Müller,[4] Georges Hadziioannou,[2] Ilias Iliopoulos,[5] Guillaume Fleury[2,*] and Marc Zelsmann[3,*]*

[1] ARKEMA FRANCE, GRL, Route Nationale 117, BP34 64170 Lacq, France.

[2] Univ. Bordeaux, CNRS, Bordeaux INP, LCPO, UMR 5629, F-33600, Pessac, France.

[3] Univ. Grenoble Alpes, CNRS, CEA/LETI Minatec, LTM, 38000 Grenoble, France.

[4] Georg-August Universität Göttingen, Institute for Theoretical Physics, 37077 Göttingen, Germany.

[5] Laboratoire PIMM, Arts et Métiers Institute of Technology, CNRS, Cnam, HESAM Université, 151 Boulevard de l'Hôpital, 75013 Paris, France.

*Correspondence to: xavier.chevalier@arkema.com ; guillaume.fleury@u-bordeaux.fr ; marc.zelsmann@cea.fr

This PDF file includes:

Figures S1 to S7

Tables S1 to S3

Supplementary Note S1

SUPPLEMENTARY FIGURES

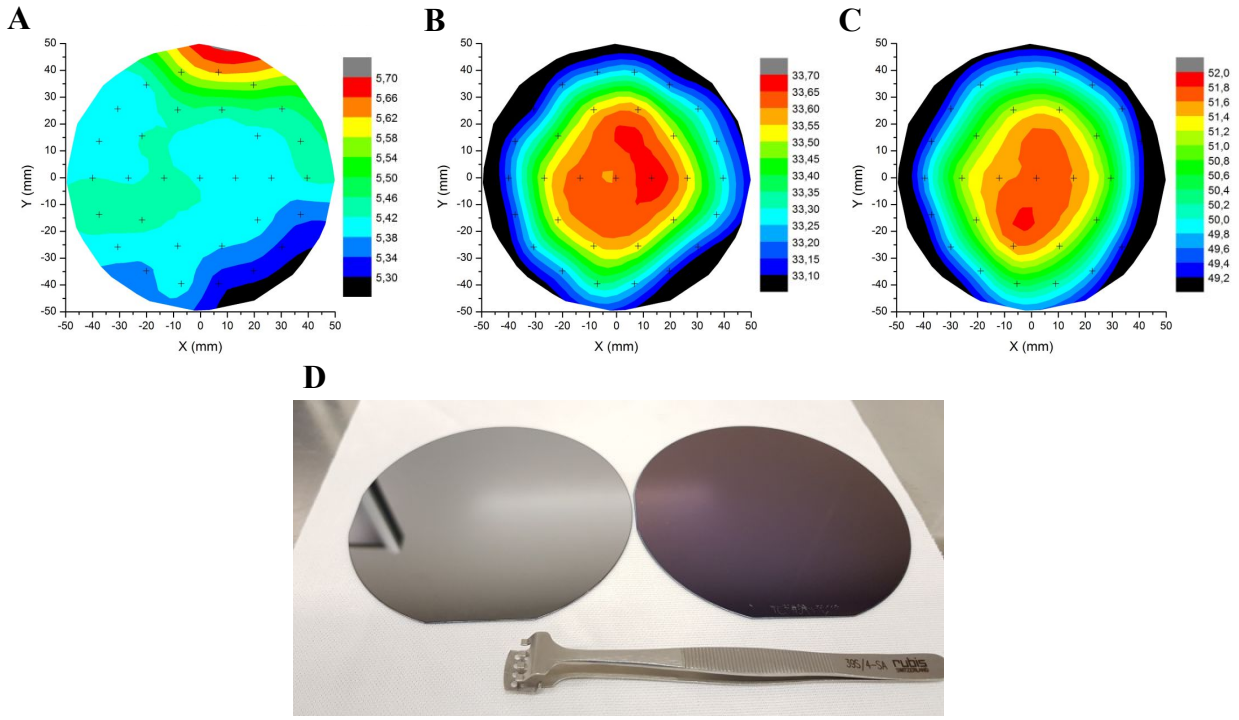

Figure S1. Detailed analysis of uniformity mapping. (**A**,**B**,**C**)Thickness uniformity map obtained by variable angle spectroscopic ellipsometry with 31 recorded data points distributed over the whole 4 inches wafer. Film thicknesses are indicated in nm. (**A**) FGH-47 NL thickness uniformity after grafting (200°C, 75 s) and rising with propylene glycol methyl ether acetate (PGMEA). (**B**) BCP thickness uniformity on the grafted NL layer after spin-coating and drying at 60°C during 60 s. (**C**) FGH-37 TC thickness uniformity on top of the NL/BCP stack after cross-linking (90°C, 3 min) and thermal annealing (240°C, 5 min) treatments. The color scale bar allows the visualization of the thickness variation over the 4 inches wafer surface. (**D**) Picture of 4-inches wafers coated with (left) an as-cast 30 nm thick L-DBS18 layer on top of a grafted NL layer after drying (60°C, 60 s) and (right) a NL/L-DBS18/TC stack after thermal annealing (240°C, 5 min), used for uniformity mapping in **B**) and **C**) respectively.

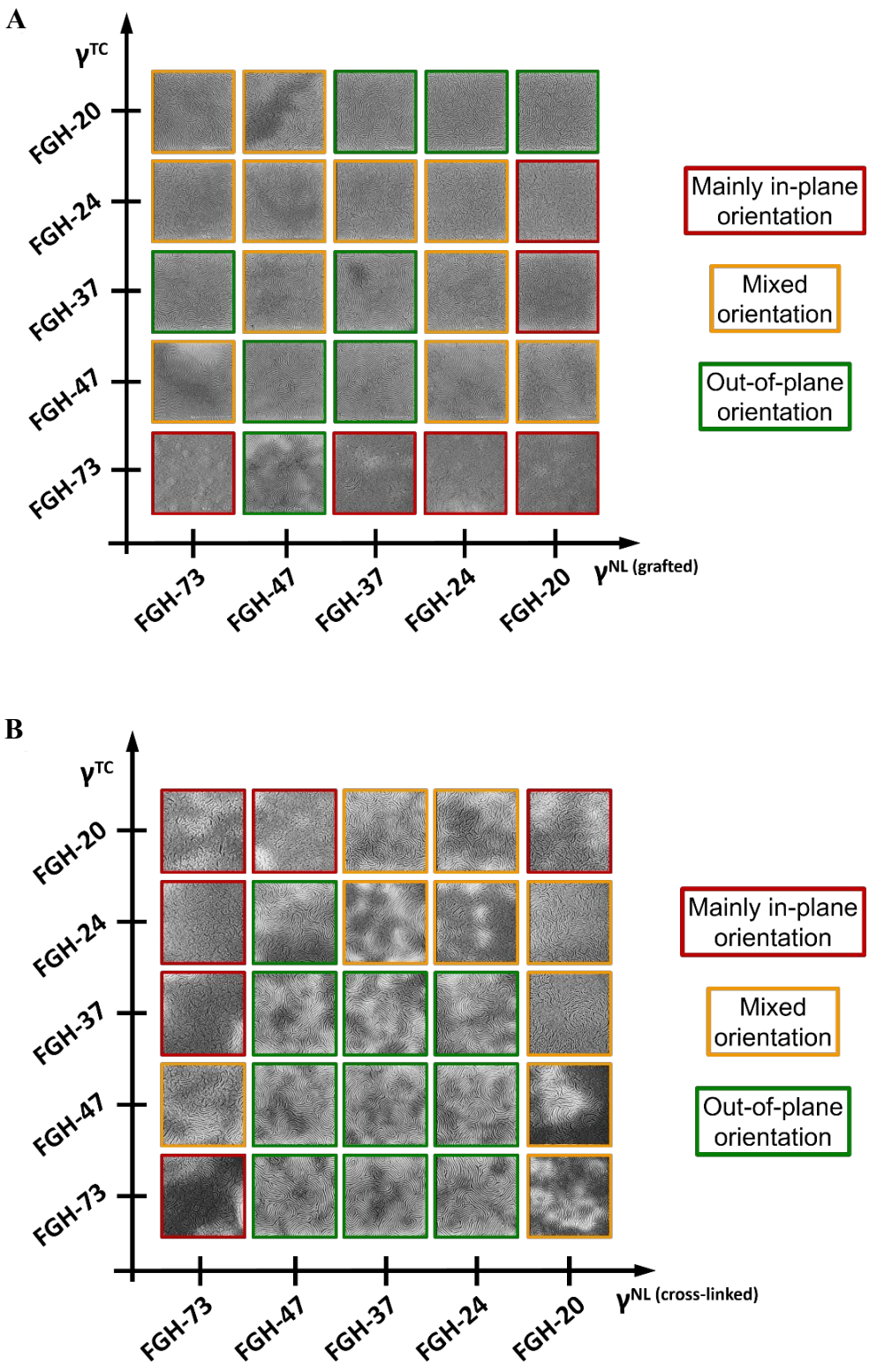

Figure S2. Detailed self-assembly cartographies related to Figure 1d,e for a 30 nm thick L-DBS18 coated on (**A**) grafted or (**B**) thermally cross-linked FGH underlayers for cross-linked TCs (UV-

365 nm, 100 mJ/cm²) with varying composition. A thermal annealing step at 260°C for 5 minutes was performed after the TC cross-linking to promote the BCP self-assembly.

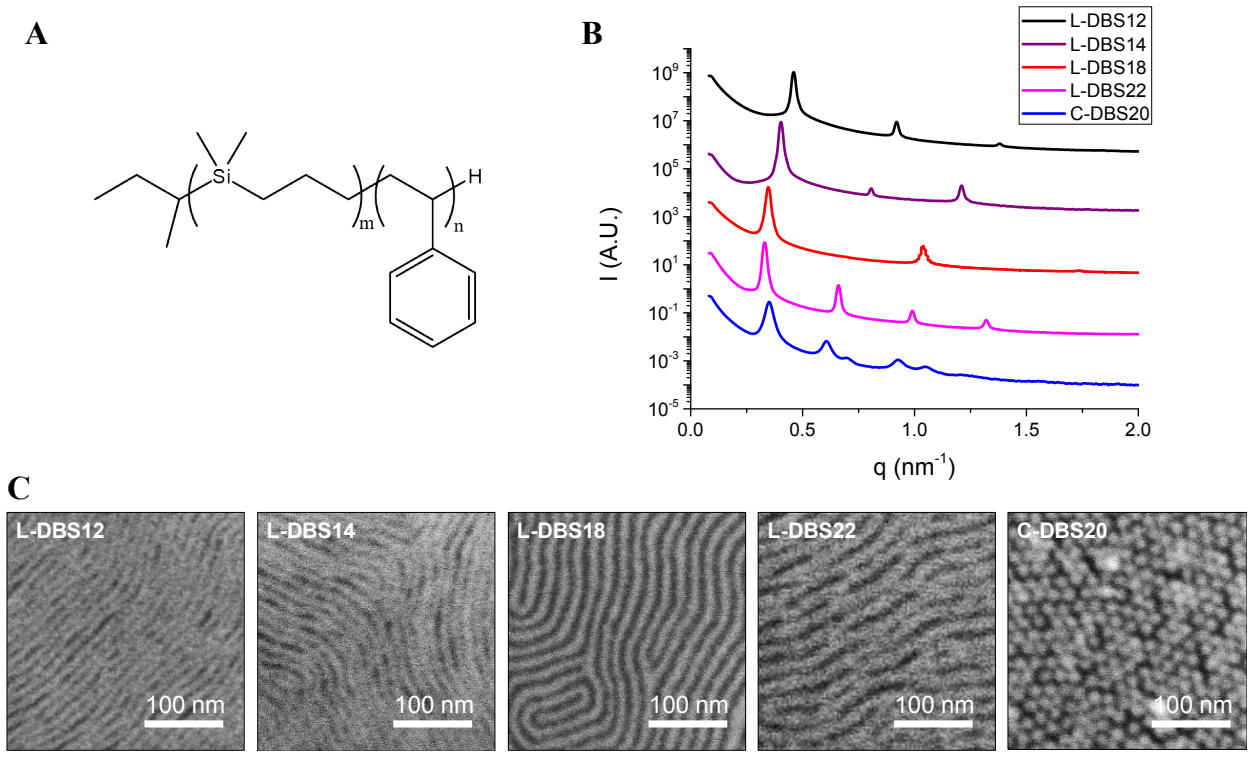

Figure S3. (**A**) Chemical structure of the poly(1,1-dimethyl silacyclobutane)-*block*-poly(styrene) BCP used in this study. (**B**) Synchrotron SAXS profiles of DBS samples obtained at 140°C. Lamellae (q/q^* = 1, 2, 3) identified with L-DBS12, L-DBS14, L-DBS18 and L-DBS22 and hexagonal phase (q/q^* = 1, √3, √4, √7, √9) identified with C-DBS20. The missing (200) reflection for L-DBS18 is attributed to the extinction of the lamellar form factor for a symmetric composition. Curves have been shifted vertically for clarity. (**C**) Nanostructured DBS thin films after thermal annealing (240°C, 5 min). Samples were imaged by SEM after TC removal and a phase contrast enhancement by plasma treatment.

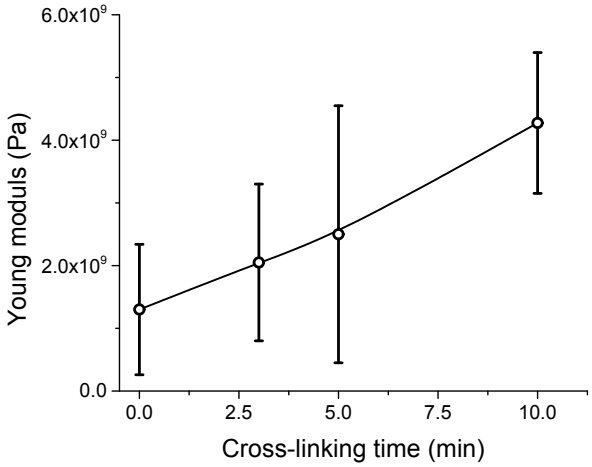

Figure S4. Evolution of the Young modulus of a L-DBS18/FGH-37 TC stack measured by AFM nano-indentation as function of the cross-linking time at 90°C.

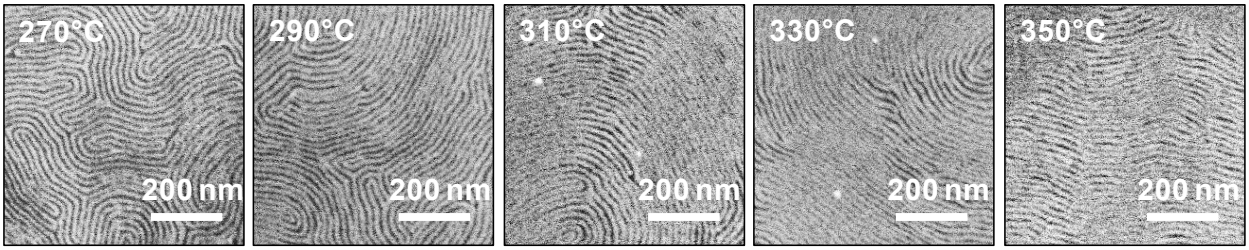

Figure S5. SEM images of nanostructured L-DBS18 thin films after rapid thermal annealing using a rapid thermal processing tool with a heating rate of 10°C.s^{-1} followed by a 30 s isotherm at the set temperature for self-assembly. Lamellar grains with improved correlation length along with the set temperature for self-assembly are observed without any dewetting of the DBS layer.

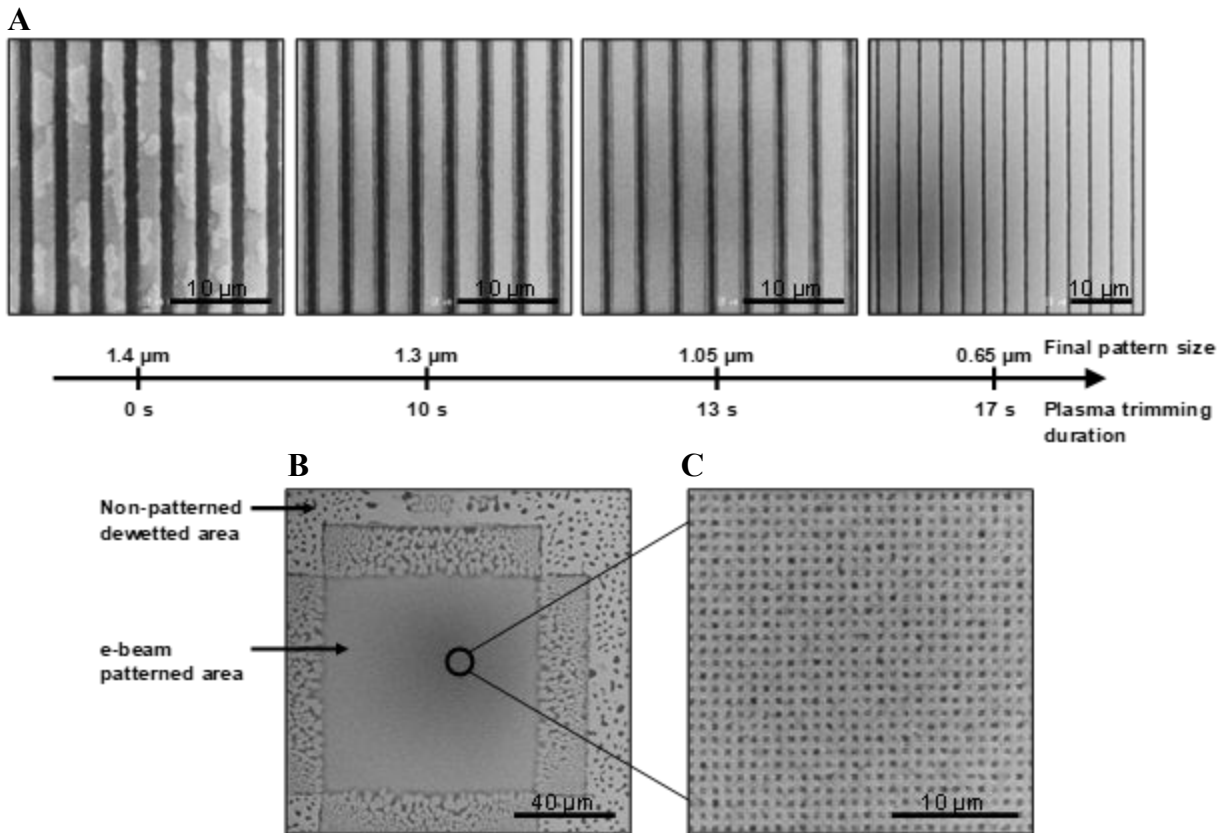

Figure S6. (**A**) SEM images of the TC-patterned areas on the samples, showing a dewetted configuration for the BCP outside the TC-patterns. The dewetted material is etched away with a non-selective plasma. The patterned areas can be further trimmed with the same plasma to further reduce their width. (**B**) low magnification and (**C**) higher magnification SEM images of a BCP/TC stack patterned with e-beam, showing a dewetted film outside the patterned area, while the whole BCP film remains flat inside the patterned area, despite the latter contains both TC-covered and uncovered areas. From (**A**) and (**C**), where the distance between two patterns is of ~2.3 µm for the dewetted film, and 500 nm without dewetting, it is deduced that the wavelength of capillary waves is located in-between these two values for the DBS system.

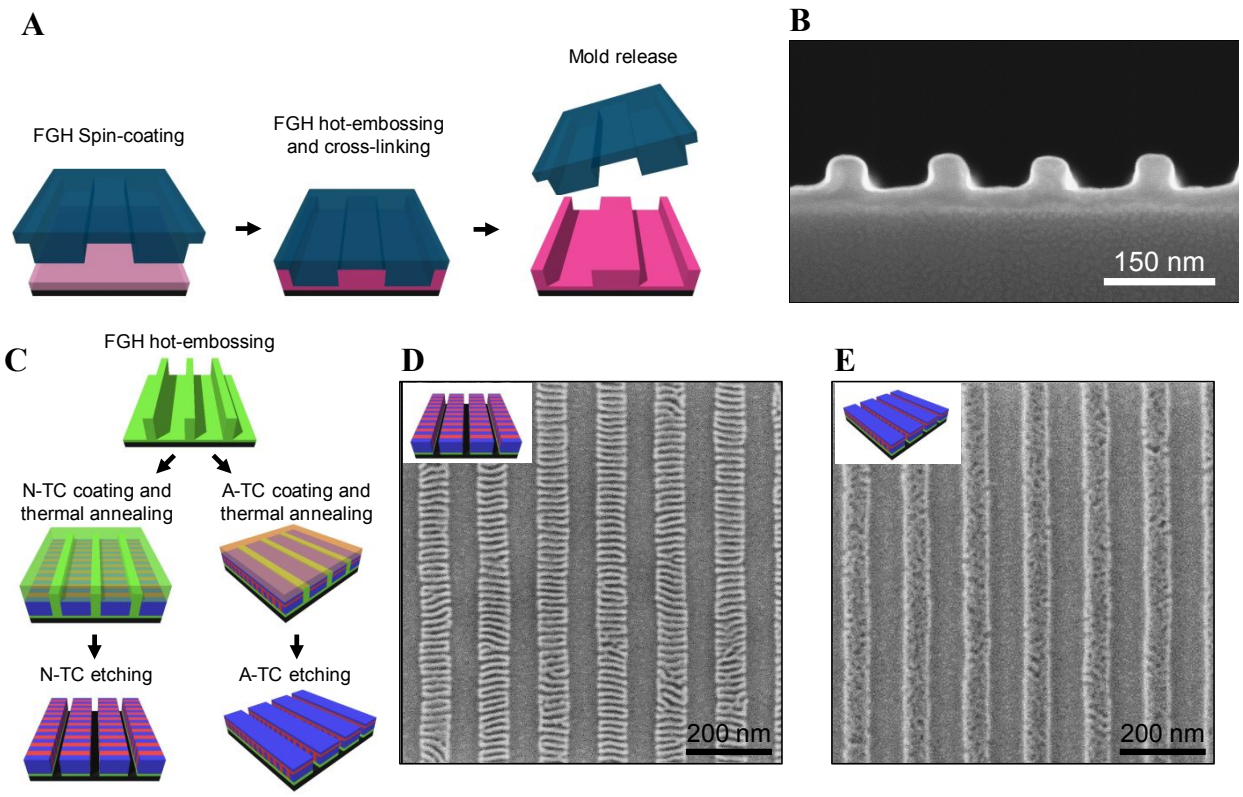

Figure S7. (**A**) Scheme depicting the fabrication of topographical templates by nanoimprint lithography of FGH layer using hot-embossing. (**B**) SEM cross-section image of the topographical template obtained following this process (85 nm wide gratings with 45 nm depth). (**C**) Schematic integration scheme illustrating the use of the N-TC and A-TC in combination with a graphoepitaxy template, obtained by hot-embossing of FGH material, for DSA to obtain perpendicular or parallel areas. (**D**) SEM top-view image of the typical ladder pattern formed by the lamellar BCP structure due to the neutral boundary conditions at the interfaces achieved by coating an N-TC (FGH-37) on top of the BCP layer. (**E**) SEM top-view image of the in-plane lamellar structure resulting from the coating of an A-TC (FGH-20) on top of the BCP templated layer.

The FGH-47 platform was used as a cross-linked underlayer patterned via nanoimprint lithography through hot-embossing to generate 85 nm wide gratings (Figure S7A,B) which were subsequently employed as graphoepitaxy templates (Figure S7C). Further coating and cross-linking of a FGH-37 N-TC on top of a L-DBS18 layer spin-coated on this patterned substrate, followed by the promotion of self-assembly through thermal annealing at 240°C, results in a typical ladder pattern for the lamellae ((Figure S7D) due to the neutral boundary conditions insured

at all interfaces. The orientation switches to parallel lamellae with the use of a FGH-20 A-TC coated on top of the BCP, as the neutral sidewalls are not “attractive” enough for the BCP to counter-balance the stronger affine surface-field arising from the A-TC (Figure S7E).

SUPPLEMENTARY TABLES

Table S1. Macromolecular characteristics of the FGH terpolymers.

TC materials	f_{GMA}[(a)]	f_{HEMA}[(a)]	$f_{MATRIFE}$[(a)]	M_n (kg.mol^{-1})[(b)]	**D**[(b)]
FGH-20	0.19	0.61	0.20	2.1	1.6
FGH-24	0.2	0.56	0.24	3.05	1.7
FGH-37	0.26	0.37	0.37	2.7	1.9
FGH-47	0.27	0.26	0.47	2.8	1.9
FGH-73	0.27	0	0.73	2.8	1.9

[(a)] Determined by ^{1}H-NMR in $CDCl_3$.

[(b)] Determined by SEC using THF as eluent at 40°C with poly(styrene) standards.

Table S2. Macromolecular characteristics of the DBS copolymers.

Name	**M_n (kg.mol^{-1})[(a)]**	**D[(a)]**	**f_{PDMSB}[(b)]**	**Morphology[(c)]**	**L_0 (nm)[(c)]**
L-DBS22	23.1	1.19	0.51	Lamellar	22
L-DBS18	17.2	1.11	0.50	Lamellar	18
L-DBS14	13.8	1.06	0.50	Lamellar	14
L-DBS12	12.0	1.09	0.48	Lamellar	12
C-DBS20	20.5	1.06	0.23	Cylindrical	20

[(a)] Determined by SEC using THF as eluent at 40°C with universal calibration technique.

[(b)] Determined by ^{1}H-NMR in $CDCl_3$.

[(c)] Determined by SAXS at 140°C.

Table S3. Surface energy of the FGH materials for both grafted and cross-linked layers. (γT: Total surface energy; γD: Dispersive component; γP: Polar component). Contact angles were measured with water, diiodo-methane and ethylene glycol respectively in order to calculate surface free energy using the Owens, Wendt, Rabel and Kaelble method.

Configuration	**Sample**	**γ^T (mN/m)**	**γ^D (mN/m)**	**γ^P (mN/m)**
Grafted layer	FGH-20	42.2	36.7	5.5
	FGH-24	36.5	31.7	4.8
	FGH-37	35	32.3	2.7
	FGH-47	33.5	30.4	3.1
	FGH-73	28.2	27.1	1.1
Cross-linked layer	FGH-20	39.7	34.6	5.1
	FGH-24	36.5	30.2	6.3
	FGH-37	32.0	27.6	4.4
	FGH-47	28.6	25.1	3.5
	FGH-73	24.6	22.7	1.8

SUPPLEMENTARY NOTE S1: DEWETTING OF NANOSTRUCTURED BCP FILMS ON "NEUTRAL" LAYERS

The wetting of BCP layers in the course of self-assembly by thermal or solvent vapor annealing is an essential aspect for the implementation of nanotechnologies based on the segregation behavior of BCPs in a thin film configuration. Extensive work performed over the past decades highlighted the main parameters that dictate the thermodynamic stability and the triggering of dewetting of homopolymer films, coated on functionalized substrates. The reader is referred to already existing excellent reviews published on the topic.[1,2] We report here the main characteristics of dewetting in the context of DSA. Among these parameters, the intrinsic nature of the substrate and the film thickness appeared to be critical ones. Regarding the nature of the substrate, the dewetting of a given homopolymer can be either favored or a film can be stabilized, depending on the nature of the physico-chemical interactions between the homopolymers and the substrate.[3]

For nanotechnology applications, the film thickness is typically much smaller than the capillary length, *i.e.*, thin films are not stabilized by gravity. First, we consider the equilibrium wetting behavior of a homopolymer on a substrate "i" that is dictated by the sign and value of the corresponding spreading parameter, *S*, defined by:

$$S_{hP} = \gamma_i - \gamma_{hP} - \gamma_{hP/I} \quad \textbf{(1)}$$

Where:

- S_{hP}: spreading parameter of the homopolymer material on the substrate i
- γ_i: surface energy of the substrate
- γ_{hP}: surface energy of the homopolymer

- $\gamma_{hP/i}$: interfacial tension between the homopolymer and the substrate

According to Young's law, the interfacial tension between the homopolymer and the substrate is expressed as:

$$\gamma_{hP/i} = \gamma_i - \gamma_{hP}.\cos\theta_{hP/I} \quad \textbf{(2)}$$

where $\theta_{hP/i}$ is the contact angle that a macroscopic drop of homopolymer forms on the substrate.

For $S < 0$, the system is thermodynamically unstable and the homopolymer will dewet the substrate. Conversely, for $S \geq 0$, the homopolymer is able to wet the substrate. This latter case only occurs for $\theta_{hP/i} = 0$, indicating a strong affinity between the substrate and the homopolymer.

As an example, we consider a homopolymer film coated onto a grafted homopolymer brush of the same constituent. In the absence van-der-Waals interactions, the homopolymer will dewet the brush (autophobicity) if the brush is densely grafted or the homopolymers are long because there is an entropic penalty for the homopolymers to enter the brush (dry-brush regime). This gives rise to a positive interface tension between brush and melt.[4] Such a configuration is thus characterized by $S \approx 0$, or S slightly negative for the autophobic case, instead of $S > 0$. Accounting for long-range van-der-Waals interactions gives rise to a complex wetting diagram.[5]

The behavior of a BCP (even for a simple diblock architecture) is more complex and only incompletely understood. An excellent recent review of Brassat and Lindner exhaustively compiles recent studies on various aspects of copolymer thin films and droplets[6] but the dewetting

of BCP/NL stacks is hardly treated. An important difference between BCP and homopolymer films is the contribution of the internal, self-assembled morphology to the interface potential, which is the film-thickness-dependent generalization of the spreading parameter. If the substrate prefers a BCP block, the morphology will adopt a parallel orientation. This layering will increase the interface potential, whenever the film thickness is incompatible with the optimal layer spacing (intrinsic period). For a BCP film with a free, deformable surface, this effect will give rise to a quantization of the BCP film thickness according to its intrinsic period, *i.e.*, the formation of holes/islands features, to minimize the free energy of the system. However, as seen on our own data (Figure 3a – the "solid/liquid" configuration with ~10% BCP coverage) this mechanism is not efficient for perpendicular morphologies.

As the BCP thickness is arbitrarily set due to application constraints and the rigid top coating does not allow for the formation of holes/islands features, the rigidity of the BCP top coat eliminates this mechanism of reducing the thickness frustration of parallel morphologies. Thermodynamically, this destabilizes parallel morphologies against dewetting and favors perpendicular structures.[7,8]

In the following, we aim to clarify some of the aspects of the NL/BCP configuration, in order to apprehend its implications in the particular framework of DSA. We assume that the top surface of the BCP layer is neutral for the BCP domains, in order to obtain a perpendicular orientation of the morphology.

The DSA based on BCPs for patterning or microelectronic applications presents some specific characteristics that will affect the wetting behavior of the BCP layer. Among these, two are especially detrimental to the thin-film stability:

i) a grafted or cross-linked neutral layer (NL) is used to balance the interfacial interactions of each domain of the BCP structure with the substrate.

ii) the BCP layer thickness is only a few tens of nm.

The NL consists of a polymer brush, typically grafted to the substrate. For an optimal pattern transfer, semiconductor industry requests a small thickness of the NL layer (≈ 5 nm or even thinner). Thus the grafted chains of the NL are often shorter than the BCPs, favoring dry-brush behavior[4] and concomitant autophobic dewetting. Moreover, if the grafting density or molecular weight of the NL were small, as to enter the wet-brush regime and eliminate the positive brush-BCP interface tension, the BCP would also interact with the selective bare substrate, compromising the neutrality of the substrate.

Additionally, the chemical composition of the NL has to be taken into consideration as regard to the wetting of a BCP layer. The chemical architecture of the NL can be either similar to the BCP ones (*e.g.*, P(S-*stat*-MMA) statistical copolymer used to control the self-assembly of PS-*b*-PMMA BCPs) or different from the BCP repeating units, without specific attractive interactions between them (*i.e.*, a *negative* χ parameter). In both cases, the presence of a constituent presenting a repulsive interaction (*i.e.* a *positive* χ parameter) for a given block (*e.g.* the MMA unit of the NL with regard to the S unit of the BCP), yields an additional enthalpic cost for the BCP segment to penetrate into the brush layer, and thus destabilizes the BCP film against dewetting. As discussed by Ganesan and co-workers,[9] this destabilization is modulated by the blockiness of the random copolymer layer. The mutual interaction BCP/NL results in a restructuring of the NL, exposing the most appropriated component at the brush-BCP interface, in order to provide a more energetically favorable situation, while still being “neutral”.

Under neutral boundaries conditions, the dewetting of the BCP occurs on the NL due to both entropic and enthalpic penalties for the blocks to interdigitate into the NL material, as long as attractive interactions are absent to counter-balance the intrinsic entropic penalty. In the case of a BCP coated on a NL of similar chemical constituents, the expression of the spreading parameter is directly derived from Eq. **(1)**:

$$S_{BCP} = \gamma_i - \gamma_{BCP} - \gamma_{BCP/i} \quad \textbf{(3)}$$

where:

- S_{BCP}: spreading parameter of the BCP on the substrate i
- γ_i: surface energy of the substrate
- γ_{BCP}: surface energy of the BCP
- $\gamma_{BCP/i}$: interfacial tension between the BCP and the substrate

Considering the neutral boundaries conditions for A_m-*b*-B_n copolymer (where m and n are the degree of polymerization of the A and B blocks, respectively), we obtain:

- For a perpendicular morphology and a neutral top surface, the surface free energy can be approximated by the weighted mean of the surface energy of each block, on the macroscopic scale. $\gamma_{BCP} = f_A.\gamma_A+f_B.\gamma_B = ½ (\gamma_A+\gamma_B)$ for a lamellar BCP (where f_A and f_B are the volume fraction of the A and B blocks, respectively).
- $\gamma_i \approx f_A.\gamma_A+f_B.\gamma_B = ½ (\gamma_A+\gamma_B)$, where we have assumed that the NL is a symmetric brush comprised of the same components as the BCP. Here we have ignored the additional free energy cost of the brush to form a narrow top surface and have neglected the

ability of the NL to rearrange as to enrich the component with the lower surface tension at the top.

- $\gamma_{BCP/i} = \gamma_{A/i} = \gamma_{B/i}$ due to the non-preferential interactions of each domain with the substrate with $\gamma_{A/i}$, $\gamma_{B/i}$, the interfacial tension of A and B blocks with the brush substrate, respectively. Analog to the autophobicity of a homopolymer, the entropic penalty of the blocks of the BCP to penetrate into the brush NL gives rise to a positive value in the dry-brush regime, even if the NL perfectly rearranges to expose the corresponding BCP component at the brush-BCP interface.

Then, the spreading parameter takes the form:

$$S_{BCP} = \gamma_i - \gamma_{BCP} - \gamma_{BCP/i} = \tfrac{1}{2}(\gamma_A+\gamma_B) - \tfrac{1}{2}(\gamma_A+\gamma_B) - \gamma_{BCP/i} = -\gamma_{BCP/i} = -\gamma_{A/i} \quad \textbf{(4)}$$

Therefore, the spreading parameter, S_{BCP}, for such configuration is negative and an A_m-*b*-B_n BCP coated on a NL containing A and B repeating units is a thermodynamically unstable system if long-range contributions can be ignored. Thus van-der-Waals interactions are the only forces, when favorable, able to stabilize the BCP against dewetting. As a result, without a tedious design and selection of the constituents of the materials (both NL and the BCP systems) to obtain such a favorable van-der-Waals contribution, while simultaneously satisfying a similar surface energy at self-assembly temperature for the blocks of the BCP to obtain the perpendicular orientation of features, the integrity of the BCP film will be jeopardized as regard to its wetting of the substrate. The pioneering study of Mansky *et al.* dedicated to the surface neutralization for the PS-*b*-PMMA system provides striking evidence of such behavior.[10] In this work, forming the basis of substrate functionalization to balance interfacial tensions, the PS and PMMA homopolymers are only

metastable on their chemically similar brushes. However, this metastable state becomes actually unstable when these homopolymers are coated onto P(S-*stat*-MMA) grafted layers, *i.e.*, both homopolymers actually dewet on the grafted NL exhibiting a neutral composition for the BCP. The demonstration of the dewetting of PS-*b*-PMMA thin films on their NLs was established afterwards.[11,12]

In the case of a NL composed of repeating units that are chemically distinct from the BCP, additional parameters have to be taken into account. Indeed, the enthalpic contribution arising from repulsive or attractive interactions between each of the NL constituents and each of the BCP segment has to be accounted for in the definition of $\gamma_{BCP/i}$.

On the one hand, repulsive interactions destabilize the BCP film by adding a positive enthalpic contribution to $\gamma_{BCP/i}$ and thereby decreasing the thermodynamic stability of the BCP film.

On the other hand, attractive interactions could stabilize the BCP layer and lead to the desired $\theta_{BCP/i} = 0$. These interactions yield a negative enthalpic contribution to $\gamma_{BCP/i}$, favoring the interdigitation of the BCP chains into the NL material and thus its stabilization with respect to dewetting once balancing the associated entropic penalty. However, it is noteworthy that even if such strong interactions were established between the NL and the BCP domains (with the same amplitude for each block due to neutrality conditions), autophobic dewetting of the BCP chains located on top of a strongly anchored BCP layer could still occur as observed by Epps *et al.*[13]

Thermodynamically, the dewetting of a BCP film on top of a NL can therefore be considered as a typical case within DSA conditions, in analogy to the autophobic dewetting of homopolymers. To circumvent this dewetting situation, the user must overcome both autophobic dewetting (entropy-

dominated interfacial energy contribution) and enthalpic penalties originating from repulsive interactions with the NL constituents.

Instead of requiring that the BCP film on the NL layer is *thermodynamically* stable, we can merely require that it is *kinetically* stable against dewetting. In the ultraclean environment of semiconductor fabrication, there are no external impurities (*e.g.*, dust) to nucleate holes in a metastable BCP film. Therefore we only need to consider the stability of the BCP film with respect to spinodal dewetting, *i.e.*, the spontaneous growth of film thickness variations. Spinodal dewetting is dictated by the curvature of the interface potential that, in turn, is chiefly determined by the thickness-dependent, long-range van-der-Waals interactions of the layers, bare substrate, NL, BCP film, (top coat), and air.

In the framework of DSA, the BCP film thickness is deliberately kept small due to pattern transfer and self-assembly constraints. Indeed, thick BCP films with high aspect ratio features are difficult to transfer into the substrate due to loading and collecting angle effects during the plasma-etch step (Aspect Ratio Dependent Etching – "ARDE"),[14] and due to pattern-collapse issues. Besides, such thick films require a more important annealing budget in order to optimize their self-assembly.[15] As a result, thin (15-30 nm) BCP films usable for DSA are entirely subject to van-der-Waals contributions, either stabilizing the film or favoring dewetting, depending on the intrinsic chemical constitution of the materials.

The interplay of long-range contributions of the different layers to the interface potential is intricate, but a judicious choice of materials may kinetically stabilize the BCP film against dewetting. This requirement, however, adds additional constraints onto the materials selection. In our work, instead, we suggest a more robust strategy: we kinetically stabilize the BCP film against

spinodal dewetting by using a crosslinked top coat whose rigidity suppresses variations of the film thickness.

References

(1) Geoghegan, M.; Krausch, G. Wetting at Polymer Surfaces and Interfaces. *Prog. Polym. Sci.* **2003**, *28* (2), 261–302. https://doi.org/10.1016/S0079-6700(02)00080-1.

(2) Gentili, D.; Foschi, G.; Valle, F.; Cavallini, M.; Biscarini, F. Applications of Dewetting in Micro and Nanotechnology. *Chem. Soc. Rev.* **2012**, *41* (12), 4430. https://doi.org/10.1039/c2cs35040h.

(3) Reiter, G. Dewetting of Thin Polymer Films. *Phys. Rev. Lett.* **1992**, *68* (1), 75–78. https://doi.org/10.1103/PhysRevLett.68.75.

(4) Matsen, M. W.; Gardiner, J. M. Autophobic Dewetting of Homopolymer on a Brush and Entropic Attraction between Opposing Brushes in a Homopolymer Matrix. *J. Chem. Phys.* **2001**, *115* (6), 2794–2804. https://doi.org/10.1063/1.1385557.

(5) Müller, M.; MacDowell, L. G. Wetting of a Short Chain Liquid on a Brush: First-Order and Critical Wetting Transitions. *Europhys. Lett.* **2001**, *55* (2), 221–227. https://doi.org/10.1209/epl/i2001-00403-3.

(6) Brassat, K.; Lindner, J. K. N. Nanoscale Block Copolymer Self-Assembly and Microscale Polymer Film Dewetting: Progress in Understanding the Role of Interfacial Energies in the Formation of Hierarchical Nanostructures. *Adv. Mater. Interfaces* **2020**, *7* (5), 1901565.

https://doi.org/10.1002/admi.201901565.

(7) Russell, T. P.; Menelle, A.; Anastasiadis, S. H.; Satija, S. K.; Majkrzak, C. F. Unconventional Morphologies of Symmetric, Diblock Copolymers Due to Film Thickness Constraints. *Macromolecules* **1991**, *24* (23), 6263–6269. https://doi.org/10.1021/ma00023a032.

(8) Kikuchi, M.; Binder, K. Microphase Separation in Thin Films of the Symmetric Diblock-copolymer Melt. *J. Chem. Phys.* **1994**, *101* (4), 3367–3377. https://doi.org/10.1063/1.467584.

(9) Trombly, D. M.; Pryamitsyn, V.; Ganesan, V. Self-Assembly of Diblock Copolymer on Substrates Modified by Random Copolymer Brushes. *Macromolecules* **2011**, *44* (24), 9867–9881. https://doi.org/10.1021/ma202075d.

(10) Mansky, P.; Lui, Y.; Huang, E.; Russell, T. P.; Hawker, C. J. Controlling Polymer-Surface Interactions with Random Copolymer Brushes. *Science* **1997**, *275* (5305), 1458–1460. https://doi.org/10.1126/science.275.5305.1458.

(11) Farrell, R. A.; Kehagias, N.; Shaw, M. T.; Reboud, V.; Zelsmann, M.; Holmes, J. D.; Sotomayor Torres, C. M.; Morris, M. A. Surface-Directed Dewetting of a Block Copolymer for Fabricating Highly Uniform Nanostructured Microdroplets and Concentric Nanorings. *ACS Nano* **2011**, *5* (2), 1073–1085. https://doi.org/10.1021/nn102720m.

(12) Ferrarese Lupi, F.; Giammaria, T. J.; Miti, A.; Zuccheri, G.; Carignano, S.; Sparnacci, K.; Seguini, G.; De Leo, N.; Boarino, L.; Perego, M.; et al. Hierarchical Order in Dewetted Block Copolymer Thin Films on Chemically Patterned Surfaces. *ACS Nano* **2018**, *12* (7),

7076–7085. https://doi.org/10.1021/acsnano.8b02832.

(13) Epps, T. H.; DeLongchamp, D. M.; Fasolka, M. J.; Fischer, D. A.; Jablonski, E. L. Substrate Surface Energy Dependent Morphology and Dewetting in an ABC Triblock Copolymer Film. *Langmuir* **2007**, *23* (6), 3355–3362. https://doi.org/10.1021/la062707q.

(14) Wu, B.; Kumar, A.; Pamarthy, S. High Aspect Ratio Silicon Etch: A Review. *J. Appl. Phys.* **2010**, *108* (5), 051101. https://doi.org/10.1063/1.3474652.

(15) Welander, A. M.; Craig, G. S. W.; Tada, Y.; Yoshida, H.; Nealey, P. F. Directed Assembly of Block Copolymers in Thin to Thick Films. *Macromolecules* **2013**, *46* (10), 3915–3921. https://doi.org/10.1021/ma3025706.